ChemistrySelect

Research Article
doi.org/10.1002/slct.202302688

Chemistry Europe
European Chemical Societies Publishing

www.chemistryselect.org

Synthesis of Copper and Cobalt complexes with a Hydrothermal Method and Their Applications in Antibiological Activity

Qiongli Luo,[a] Lei Wang,[a] Shuangyan Wu,[a] Mingchang Zhu,[a] Ying Zhang,*[a] and Lin Lin*[b]

Two novel 2-(1,2,4-triazol-1-yl)-4-pyridyl acid complexes with $Cu(ClO_4)_2 \cdot 6H_2O$ and $Co(NO_3)_2 \cdot 6H_2O$ were synthesised and their biological activities were systematically studied in vitro. The interaction between the complex and DNA was determined by UV spectroscopy, yielding binding constants of 6.63×10^3 and 6.09×10^3, respectively. The DNA binding abilities of the complexes were also investigated using fluorescence spectroscopy, showing quenching values of 0.13 and 0.08, respectively. Agarose gel electrophoresis showed that both the copper and cobalt complexes could effectively cleave DNA. In addition, flow cytometry, cell morphology detection, and MTT assays showed that the synthesised complex induced apoptosis The experimental results show that the copper complexes have promising medicinal value as potential anticancer drugs.

Introduction

Metal coordination polymers are widely used in gas storage, catalytic activity, and molecular and biomedical fields because of their complex valence bonds and spatial structures.[1,2] Since the discovery that platinum complexes can crosslink with DNA to form platinum-DNA adducts, their antitumor activity has been extensively studied.[3,4] After platinum drugs enter cells, they can react with sulfhydryl groups on proteins and nitrogen atoms in nucleic acids, causing DNA damage and eventually leading to cancer cell necrosis or apoptosis.[5–8] However, the disadvantages of platinum drugs have also emerged, such as low bioavailability, strong drug resistance, poor water solubility and serious side effects (damage to other parts of the body, including nephrotoxicity and peripheral neurotoxicity).[9–11] In the field of antitumor drugs, metal complexes are looking for potential alternatives to platinum drugs, and copper is an indispensable nutrient element in living organisms.[12,13] As essential trace elements, cobalt and copper can bind to a variety of functional groups and effectively interact with DNA to modify proteins.[14–16] In coordination compounds, the transformation from oxidized Cu^+ to Cu^{2+} plays an important role in chemistry and is also used as a catalyst in various biochemical reactions.[17–19] At the same time, it is also involved in a variety of metabolic pathways, such as mitochondrial respiration, free radical scavenging and iron absorption.[20,21] Its toxicity is based on the direct production of reactive oxygen species (ROS) that cleave DNA and RNA, and its distribution and homeostasis can be highly regulated.[22,23] Studies suggest that copper is an essential cofactor for tumor angiogenesis, because most tumor growth and metastasis depend on angiogenesis, and angiogenesis requires a specific amount of copper.[24–26] Cobalt usually exists in the form of Co^{2+} or Co^{3+}, which can regulate the redox potential between normoxic and hypoxic tissues, and is the only d^7 ion. The common cobalt complexes are octahedral configurations, which are widely used. It can catalyze water to produce hydrogen and has potential applications in cytotoxic drugs.[27] Cobalt-containing nanoparticles have been used in various MRI contrast agents due to their diamagnetism.[28,29] It is worth noting that the reduction potential of Co-TPA synthesized by E. S. O′ Neill et al. can accurately locate the transformation of normoxia and hypoxia in vivo, whether in chronic blood vessels with poor tumor site or in acute blood blockage of heart attack, and further understand the pathology. As Co-TPA complexes are also used as carriers and cytotoxin delivery agents, Co (III) is reduced in hypoxic tissues, and this selective reduction plays a crucial role in antitumor activity.[30,31] Compared with cisplatin, copper complexes can lead to DNA damage by active substances through oxidative stress, have apoptotic characteristics in living cells,[32,33] and are less toxic than cobalt metals.

Recently, Sabiha A. Shaikh et al. reported two fluorescently-labeled copper complexes [Cu-(phen) (L) $(ClO_4)_2$] (1) and [Cu (bpy) (L) (H_2O) (ClO_4)] (ClO_4) (2), which showed good cytotoxicity to human alveolar basal epithelial cells (A549) and breast cancer cell lines (MCF-7) with half inhibitory concentrations of 159 and 160 μM, respectively.[34,35] The $[Cu (2CP\text{-}Bz\text{-}SMe)]^{2+}$ complex synthesized by Adolfo I et al. has strong cytotoxicity against human cancer cell lines A549 (5.7 μM) and MCF-7 (5.2 μM).[36] Yamini Thakur et al. reported that Np-TBHA-Co (II) and N-p-NBHA-Cu (II) exhibited anticancer activity against MCF7 and

[a] Q. Luo, Dr. L. Wang, Dr. S. Wu, Dr. M. Zhu, Dr. Y. Zhang
The Key Laboratory of the Inorganic Molecule-Based Chemistry of Liaoning Province and Laboratory of Coordination Chemistry,
Center of Physical Chemistry Test,
Shenyang University of Chemical Technology
110142 Shenyang (P. R. China)
E-mail: zhangy621@syuct.edu.cn

[b] Dr. L. Lin
Department of Pharmacology,
Shenyang medical colleges,
110034 Shenyang (P. R. China)
E-mail: linlin1986@symc.edu.cn

Supporting information for this article is available on the WWW under https://doi.org/10.1002/slct.202302688

cervical cancer cell line (SiHa), and the half inhibitory concentration values were 38.09 μM and 89.52 μM.[37] Three novel copper (II), cobalt (II), and nickel (II) complexes of juglone (Jug) containing 1,10-phenanthroline (phen) ligand were synthesized by Leila Tabrizi. [M $(Jug)_2$ (phen)] (M = Cu (II), Co (II), and Ni (II)) showed strong anticancer activity against human cervical cancer (HeLa), human liver hepatocellular carcinoma (HepG-2) and human colorectal adenocarcinoma (HT-29). The half inhibitory concentrations of cisplatin were 12.88 μM, 8.26 μM, and 6.3 μM, respectively, which were several times lower than that of cisplatin.[38] The cytotoxicity of copper complexes reported by Ma et al. was 7.2 μmol/L, and the cytotoxicity of cobalt complexes synthesized by Alina Fudulu et al. was 6.58 μM.[39,40] Based on the transition metal complexes with a variety of topological structures and excellent therapeutic properties, as well as the continued study of Bx PC-3 cytotoxicity.

Theoretically, mobility based on DNA spatial structure regulates cell function by interfering with DNA replication or regulating transcription.[41–43] This allows for an understanding of biology from a molecular perspective, explain cancer pathogenesis at the genetic level, and fully understand the pathological processes of pancreatic cancer. Inorganic medicinal chemistry is an important field in chemotherapy and diagnostics.[44] Nitrogen-containing aromatic heterocyclic ligands and ligands containing carboxylic acids hold dominant positions among diverse coordination compounds.[45,46] Different ligand structures can improve the binding strength and specificity for metal ion binding with DNA.[47,48] Owing to the advantages of monodentate, bidentate, chelating, bridging, and other coordination modes, nitrogen-containing polycyclic carboxylic acid ligands can be synthesised. Metal complexes formed by benzimidazole and imidazole ligands containing heterocyclic nitrogen compounds are important pharmacophores.[49] When the ligand forms a polymer, a hydrogen-bond recognition group is added, favouring supramolecular system formation. The π-π stacking of the aromatic ring stabilizes the supramolecular complex and imparts strong affinity for DNA. Considering these facts, 2-(1,2,4-triazole-1-yl)-4-picolinic acid was selected as the ligand and two new Cu(II) and Co(II) complexes were prepared using a hydrothermal method.

Results and Discussion

Crystal structure analysis

X-ray diffraction crystallography confirmed the structural characteristics of the two prepared complexes and the specific crystal parameters are listed in Table S1. The Cu complex belongs to the triclinic system and is located in the P-1 space group. The copper complex is a zero-dimensional polymer (Figure 1a), where one-dimensional and two-dimensional structures were obtained by hydrogen bonding. The coordination of the complex comprises six modes with four O atoms of crystalline water and two N atoms of the ligand coordinated

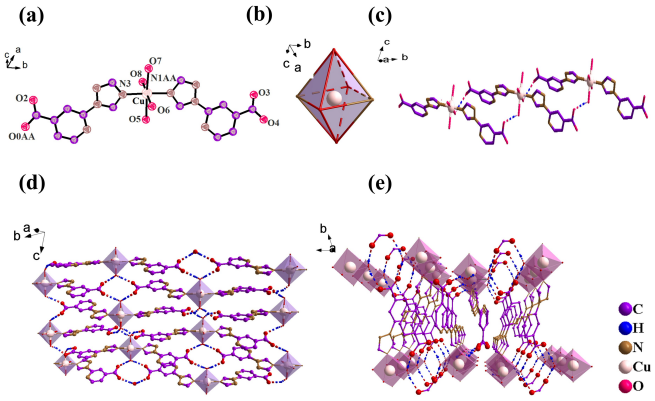

Figure 1. (a) Zero-dimensional structure of copper complex; (b) The coordination environment diagram of copper complex; (c) The 1D framework of copper complex; (d) 2D framework of copper complex; (e) Three-dimensional network structure.

with Cu to form an octahedral structure. The bond lengths and angle data for the copper complexes are provided in Table S2–3. The non-hydrogen atom coordinates and crystal parameters are provided in Table S4. The coordination environment of copper complexes (Figure 1b). The one-dimensional structure of the copper complex is connected by hydrogen bonds between O–H…O (Figure 1c). The copper complexes are connected by hydrogen bonds between O–H…O, one of which is O8 from the water molecules. The other O atom originated from the carboxylic acid group O0AA of the ligand, which was connected to form a one-dimensional chain structure. The chain complex is connected by hydrogen bonds to form a two-dimensional planar structure (Figure 1d). The donor and acceptor atoms of the hydrogen bonds are O6, O3, and O4. The donor and acceptor atoms are connected to the H atom to form a hydrogen bond, which is further connected to form a three-dimensional structure. The O atoms were more dependent than O0AA, O3, O4, O6, and O8 (Figure 1e).

The zero-dimensional structure of the cobalt complex (Figure 2a) and its coordination environment diagram were

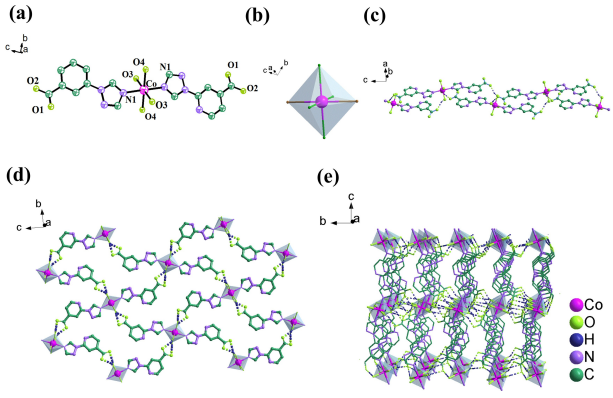

Figure 2. (a) Zero-dimensional structure of cobalt complex; (b) The coordination environment diagram of cobalt complex; (c) The 1D framework of cobalt complex; (d) 2D framework of cobalt complex; (e) Three-dimensional network structure.

determined (Figure 2b). In the one-dimensional structure of the cobalt complex (Figure 2c), the coordination mode is six-coordinated, and Co is connected to four O atoms in the crystal water and two N atoms in the ligand to form an octahedral structure. The chains of the cobalt complex formed a two-dimensional planar structure through hydrogen bonding (Figure 2d). The donor and acceptor atoms of the hydrogen bonds are O1, O2, O3, and O4, and the donor and acceptor atoms are connected to the H atom to form a hydrogen bond. Thus, the cobalt complex forms a three-dimensional structure (Figure 2e). The interaction of all hydrogen bonds can be used to obtain a three-dimensional structure diagram and the data were calculated using Platon software.

First, the structure and purity of the copper and cobalt complexes were studied by powder X-ray diffraction (PXRD; Figure S1). Through graphical comparison, it was found that the PXRD pattern of the collected powder corresponded to the simulated data, indicating that the collected powder phase was pure and could be used for subsequent experiments. The infrared spectrum of the ligand shows obvious stretching vibrations at 3430.69, 3123.10, 2473.72, and 1887.07 cm^{-1} (Figure S1c), corresponding to the intermolecular hydrogen bonds O–H, C=N, and carboxylic acid groups O–H and C–H, respectively. However, in the infrared spectra of the two complexes, the infrared vibrations at 2797.10 and 1887.07 cm^{-1} disappeared, N was involved in the coordination, while the peak intensity and hydrogen bond of the intermolecular hydrogen bond O–H increased. The thermal stabilities of the copper and cobalt complexes in a N_2 atmosphere were studied by thermogravimetric analysis (TGA). The copper complex was synthesised in methanol and water at 100 °C and excess solvent was dried and evaporated in an oven at 80 °C. The cobalt complex lost DMF molecules at a rate of 15%. The weight loss was related to the decomposition of the framework, mainly owing to the loss of coordination water and the structure further collapsed with increasing temperature (Figure S1d).

Fluorescence spectrum analysis

By tracking variations in fluorescence intensity before and after a contact, fluorescence spectroscopy may be used to investigate how tiny compounds and DNA interact. EB is a planar molecule that is only very slightly fluorescence-intensity conjugated. As a result, it may be utilized as a fluorescent probe with exceptional selectivity and high sensitivity. When integrated into DNA, the complex significantly increased its fluorescence output, emitting bright fluorescence at about 600 nm. The complex competed with the EB-DNA system after intercalation with DNA, assuming control of the DNA-binding site and releasing EB. As a result, the system was quenched and the fluorescence intensity decreased, impeding future DNA replication. The fluorescence intensity of EB-DNA steadily reduced as the complex concentration grew, demonstrating that EB may be utilized as a spectral probe to reflect the capacity of metal ions and DNA to interact.

The classical Stern-Volmer equation calculates the fluorescence quenching constant K_{SV}: $I_0/I = 1 + K_{SV} \cdot r$.[31] I_0 represents the fluorescence intensity in the absence of a quencher and I is the fluorescence intensity in the presence of a quencher. K_{SV} is the slope of the plot of I_0/I versus r. The quenching intensity was determined from the curve of I_0/I and r. The fluorescence quenching constants of the copper and cobalt complexes were 0.13 and 0.08, respectively (Figure 3). When some groove adhesives, also has a similar behavior. Therefore, the interaction of copper and cobalt complexes with DNA may occur through their grooves.[30–31] In contrast, copper complexes exhibit better affinity, which may be due to their special material composition, resulting in changes in structure and function, which may be because of their particular material makeup, leading to changes in structure and function.[32]

UV Absorption Spectroscopy

Ultraviolet spectroscopy is mainly used to track the π-π* transition of the ligand, and the binding ability of the complex to DNA is studied according to the strength of the old. The aromatic chromophore of the complex has a strong stacking effect with the base pair of DNA. Such an insertion mode depends on the binding of the metal complex to DNA, which is characterized by blue shift or red shift. Under UV irradiation, DNA molecules exhibit special structural group absorption and peak metastasis after binding to optically active target molecules. Therefore, the addition of a DNA solution to a complex solution gradually causes a change in the wavelength and strength of peaks absorption, which will be monitored to determine the hydrogen bond capacity of the metal complexes and DNA. UV radiation mainly acts on DNA, damaging its structure and reducing the ability of cells to reproduce and self-replicate.

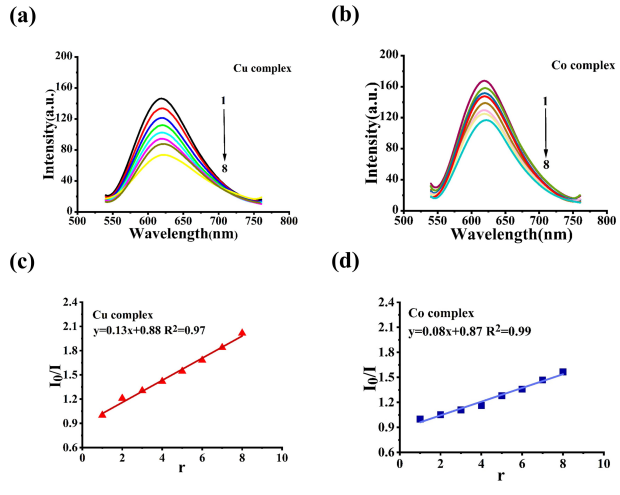

Figure 3. (a) and (b) are the emission spectra of copper and cobalt complexes competing with EtBr-DNA; (c) and (d) are the fluorescence quenching constants of copper and cobalt complexes for EB-DNA system respectively.

Copper and cobalt complexes exhibited similar absorption peaks at about 233 nm and 283 nm, respectively. With the increase of CT DNA, the characteristic absorption peaks of complexes changed. With the increase of DNA concentration, the absorption peaks at 233 nm and 283 nm were significantly higher, and the absorption peak 283 nm were blue-shifted (Figure 4). The absorbance intensity of the DNA copper complex increased from 0.210 to 0.9486, the absorption wavelength increased from 283 nanometres to 260 nm and the blue shift was approximately 23 nm. Cobalt complex complexes with DNA increased uptake from 0.154 to 0.902, wavelength from 284 nm to 260 nm and blue shift to 24 nm. This suggests that the two complexes interact with DNA through hydrogen bonds, thus enhancing the interaction between electrons. Thus, single crystals can be inserted into the base pairs of DNA through hydrogen bonding, which form hydrogen bond with the N-atoms in the complex, thus stabilizing the DNA structure. At 200–360 nm, the absorption of copper complex is stronger than cobalt complex, which was associated with the metal ligand charge transfer (MLCT) band. The UV binding constants of copper and cobalt complexes to DNA is calculated as follows: K_b:[33]

$$\frac{1}{A-A_0}=\frac{1}{A_\infty-A_0}+\frac{1}{K_b(A_\infty-A_0)}\times\frac{1}{[DNA]} \quad (1)$$

In accordance with the above formula, the binding constant were derived from the ratio of slope to intercept of 1/(A–A_0)/1/[DNA] linear graph. The binding constant K_{b1} of the copper complex is 6.63×10^3, while the binding constant K_{b2} of the copper and cobalt complexes were 6.09×10^3. This suggests that copper and cobalt complexes can be inserted into DNA, and copper complexes bind better to DNA than cobalt complexes.

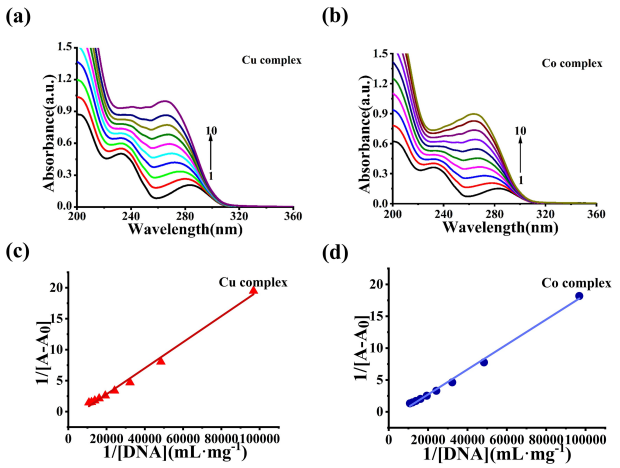

Figure 4. Copper (a) and cobalt (b) complex UV absorption spectra; (c) and (d) show the UV binding constants of the copper and cobalt complexes with CT-DNA, respectively.

DNA cleavage discussion

Supercoiled pBR322 plasmid DNA was used as a cleavage agent for DNA. In general, the interaction between DNA and proteins, and their lysis efficiency, is determined by observing the shape and extent of DNA fragmentation by agarose gel electrophoresis. Under electric field, DNA molecules are negatively charged and migrate to the anode. Factors affecting migration include agar gel density, compound concentration, voltage and buffer solution. Different DNA cleavage activities was observed when different metal ions were transferred to the supercoil. The transition from the first supercoiled form (I) to the second gap form (II) was evident, suggesting that the two complexes severed a strand of the pBR322 plasmid DNA. Both complexes cleaved pBR322 plasmid DNA. The undoped complexes were the third and seventh lanes, and the concentrations of lanes 0–2 and 4–6 were 1.25×10^{-5}, 2.5×10^{-5} and 5×10^{-5} mol/L, respectively. The concentration of the complex caused a change in the form of plasmid pBR322 dna in the lane, that is, Form (I), which decreased with the corresponding increase of Form (II). The cutting efficiency of the copper complexes was higher than that of the cobalt complexes, and the concentration gradient was more dramatic (Figure S2).

Molecular docking research

The binding mechanism and directionality of DNA and complexes can be accurately predicted by molecular docking. For this reason, a computational docking study of copper and cobalt complexes was performed to further understand the drug-DNA interactions and potential binding modes. This is a widely used process, and DNA is a commonly used receptor in drug design. The relatively large amount of DNA used in the experiment means that current computational resources are incapable of performing docking calculations. The structures of DNA1 (PDBID:4AV1) and DNA2 (PDBID:4QJU) were built using AutoDock Vina from a database of proteins (www.rcsb.org/pdb). The ligand structure was optimized in YASARA software using AutoDock (ADT) and the best binding site was identified. Genetic algorithms are used to calculate the blind docking of energy and copper-cobalt complexes bound to DNA. Copper and cobalt complexes were involved in the simulation, with minimal energy docking, their optimal conformations was inserted into adjacent DNA base pairs (Figure 5). The results show that the copper-cobalt complexes could bind to the base pairs in protein DNA to form hydrogen bonds with high affinity. The close combination of the two suggests that both Copper- and Cob alt can be used as DNA-binding metals, suggesting they may play an important role in the development of new drugs.

In vitro cytotoxicity study

The MTT assay is primarily used to measure the ability of drugs to induce apoptosis. The copper and cobalt complexes can

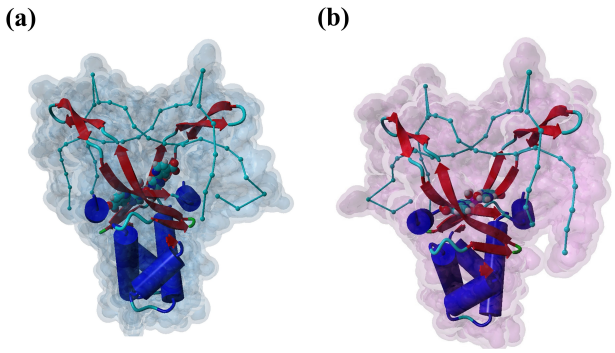

Figure 5. Docking diagrams of the copper (a) and cobalt (b) complexes with 4QJU DNA.

produce different cytotoxicities, and their induction abilities also differ (Figure 6). The percentage of living cells decreased with increasing complex concentration, indicating that the cytotoxicity of the copper and cobalt complexes was dose dependent in a linear manner. In contrast, both complexes inhibited the growth of BXPC-3 cells, whereas the copper complexes showed slightly higher cytotoxic activity. According to table S1, the toxicity of copper and cobalt complexes to BXPC-3 cells was evaluated, and the half inhibitory concentration values were 0.86 μM and 1.71 μM, respectively. It shows that the copper complex has considerable cytotoxicity to BXPC-3 cell line. In this case, the half-inhibitory concentration of oxaliplatin was 0.54 μM, indicating that the cytotoxicity of copper complexes was not significantly different from that of oxaliplatin.

Apoptosis study by flow cytometry

Normally, living cells undergo orderly division and decay to maintain balance. Once this balance is disrupted, the cells divide and multiply indefinitely, leading to disease. Therefore, the behaviour of cells affects the health of living organisms and is particularly important for measuring the anticancer activities of prospective drugs. The cells were stained with Annexin V FITC and PI, and the interactions between the copper and cobalt complexes and BxPC-3 cells were investigated using the Annexin V-FITC/PI method. Each image was divided into four quadrants and after BxPC-3 cells were treated with the copper and cobalt complexes for 24 h, the early apoptosis rates were 52.4% and 43.2%, late apoptosis rates were 19.5% and 23.7%, and total apoptosis rates were 71.9% and 66.9%, respectively (Figure 7).

The data on apoptosis induction showed that the total apoptosis rate induced by the copper complex was higher and its ability to induce apoptosis was superior to that of the cobalt complexes. In addition, annexin V-positive cells in samples treated with copper and cobalt complexes mostly appeared in the late apoptotic quadrants. This indicates that early apoptosis of cells was maintained within 24 h of incubation with the complexes.

Morphological analysis of apoptosis

Imaging technology for apoptosis mainly observes cells through changes in cell morphology. Cell imaging was performed using a fluorescence inverted microscope, observing cell morphology at a wavelength of $\lambda = 560$ nm. For example, apoptotic cells detached from the adjacent cells, the cell body became round, accompanied by cytoplasmic concentration and fold changes. In contrast, cell necrosis is caused by cell death due to severe damage and plasma membrane rupture releases contents, leading to an inflammatory response, whereas apoptosis does not break down or release the cellular contents. It is a programmed active death process that involves multiple genes and is mediated by multiple signalling pathways.

The effects of the copper and cobalt complexes on apoptosis were observed at 20×magnification. Unlike to the images of the cells incubated without the complex, the nucleus remained intact (Figure 8). After interacting with the metal complex, DAPI staining showed that the cell morphology changed. Nuclear fragmentation, chromatin condensation, and apoptotic bodies leading to apoptosis are indicated by red arrows. In the control group without complex addition, many living cells were observed after calcein staining. Many cells died due to action of this complex and both copper and cobalt complexes effectively induced apoptosis in BXPC-3 cells, while copper exhibited stronger apoptosis-inducing activity.

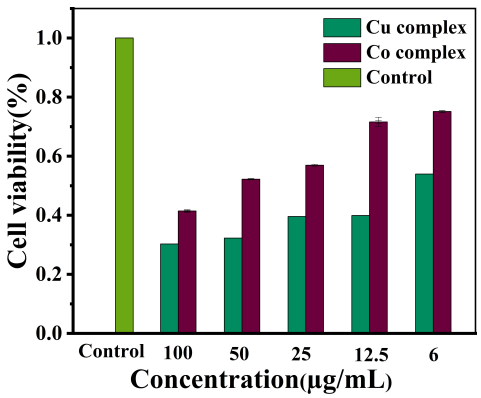

Figure 6. Cell viability curve of BxPC-3 cells treated with the prepared copper and cobalt complexes.

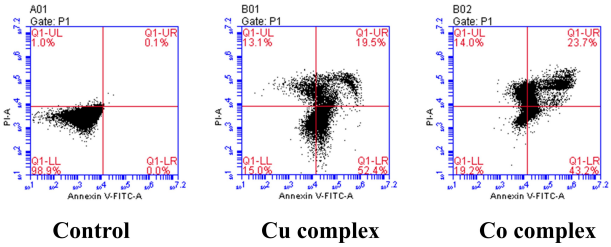

Figure 7. Flow cytometry analysis of the prepared copper and cobalt complexes incubated with BxPC-3 cells.

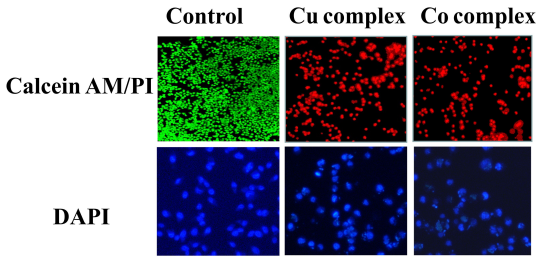

Figure 8. Apoptosis of BxPC-3 cells treated with copper and cobalt complexes for 24 h.

Conclusions

Herein, copper and cobalt complexes were synthesised using 2-(1,2,4-triazol-1-yl)-4-isonicotinic acid as a ligand, and their antitumour activities were studied. Although both copper and cobalt complexes can affect the viability of cancer cells, it was found that copper complexes exhibited the best induction of apoptosis by comparing the DNA cleavage ability, fluorescence quenching degree, and cytotoxicity, and the activity of the complex depends on the structural characteristics of the metal ions and the position of the 2-(1,2,4-triazole-1-yl)-4-picolinic acid groups. Therefore, it was determined that Cu complexes are the most promising anticancer functional materials. And the renal toxicity, nausea, vomiting, low solubility, high cross-resistance and other shortcomings of metal drugs, the design and development of low toxicity, high efficacy, good bioavailability and weak cross-resistance of copper complex is the hotspots research in the current group antitumor complexes.

Experimental Section

Chemical reagents and instruments

2-(1,2,4-triazolyl)-isonicotinic acid, $Cu(ClO_4)_2 \cdot 6H_2O$, $Co(NO_3)_2 \cdot 6H_2O$, N,N-dimethylformamide (DMF) were obtained by Sinopharm Chemical ReagentCo, Ltd. Calf thymus DNA (CT-DNA) and plasmid DNA (pBR322) were obtained from Sigma. Fluorescein isothiocyanate (FITC) and propidium iodide (PI) were purchased from BD Biosciences. Human pancreatic cancer cell (BxPC-3) was purchased from Wuhan Punosai Life Technology Co, Ltd. 2-(1,2,4-triazol-1-yl)-pyridine-4-carboxylic acid (PCA) was purchased from Jinan Henghua Technology Co,Ltd.

All fluorescence spectra were acquired using a PerkinElmer LS-55 fluorescence spectrometer equipped with a xenon lamp. The infrared spectrum was obtained in the range of 400–4000 cm^{-1} using a Nicolet Fourier transform infrared (FT-IR) 470 spectrophotometer, and UV absorption spectra were recorded using a UV-2400 spectrophotometer. The apoptosis assay was performed using a BD Accuri C6 and gel electrophoresis was performed using a JS-380A gel electrophoresis apparatus.

Synthesis of the copper complex

$Cu(ClO_4)_2 \cdot 6H_2O$ (0.18 g, 0.49 mmol) and PCA (0.062 g, 0.31 mmol) were stirred in Methanol/H_2O (2 : 1) for 2 h. The mixed solution was transferred to a 36 mL vial, reacted at 80 °C for 72 h, and slowly cooled to room temperature to obtain blue flake crystals. Yield: 79.67 % (based on the ligand). Elementary analysis (C16H18CuN8O8): C, 37.35; H, 3.50; N, 21.79; Found (%): C, 37.28; H, 3.22; N, 21.88. (Deposition Numbers 2242221 (copper complex) contain the supplementary crystallographic data for this paper. These data are provided free of charge by the joint Cambridge Crystallographic Data Centre and Fachinformationszentrum Karlsruhe Access Structures service.).

Synthesis of the cobalt complex

$Co(NO_3)_2 \cdot 6H_2O$ (0.06 g, 0.21 mmol) and 2-(1,2,4-triazole-1-yl)-4-picolinic acid (0.062 g, 0.31 mmol) were dissolved in ((DMF)/H_2O = 1 : 1) and stirred for 2 h. The mixed solution was transferred to a 36 mL vial, reacted at 80 °C for 72 h, and slowly cooled to room temperature to obtain pink crystals. Yield: 63.58 % (based on the ligand). Elementary analysis ($C_{16}H_{18}CoN_8O_8$): C, 37.70; H, 3.53; N, 21.99; Found (%): C, 37.76; H, 3.49; N, 21.96. (Deposition Numbers 242283 (cobalt complex) contain the supplementary crystallographic data for this paper. These data are provided free of charge by the joint Cambridge Crystallographic Data Centre and Fachinformationszentrum Karlsruhe Access Structures service.).

X-ray crystallography analysis

The single crystal X-ray data of copper and cobalt complexes were collected by Bruck smart 1000 CCD diffractometer at room temperature, and scanned at ω-2θ in the form of single crystal. The structure was analyzed by the standard direct method (SHELXS), and the SHELXTL software package was improved by the least square method on F^2. In the final cycle, the non-hydrogen atom coordinate anisotropic thermal parameters were further refined. First, according to the position of all metal atoms, finding the oxygen and carbon atoms of the compound in the differential Fourier diagram, and then the hydrogen atoms of the organic ligand generated through the Olex2 program.

Fluorescence spectroscopic studies

The fluorescence spectra were measured at an excitation wavelength of 526 nm. The experiments were performed in a Tris-HCl/NaCl hydrochloric acid buffer solution (pH 7.4). 50 mmol/L Tris-HCl buffer solution, 5×10^{-5} mol/L DNA, EtBr and metal complex solution were prepared. To 2 mL of the prepared DNA solution, 0.4 mL of the bromide (EB) solution was added and left to stand in the dark for 2 h. Subsequently, 0, 1, 2, 3, 4, 5, 7, and 10 mL of the 5×10^{-5} mol/L complex solutions were added and diluted to 20 mL with water. The fluorescence emission spectra of the complexes were obtained after incubation in the dark for 2 h. The intensity was measured in the dark for 2 h at room temperature.

UV Absorption Spectroscopy

CT-DNA (0.018 g) was weighed and dissolved in distilled water, diluted to 500 mL, and allowed to react for 1 h. The copper and cobalt complexes were prepared in a 1.4×10^{-4} mol/L solution. The same volume of solvent used for dissolved the complex was diluted to 100 mL with Tris-HCl buffer solution. The same volume of solvent used for the complex was diluted with a Tris-HCl buffer solution and finally diluted to 100 mL. The sample and reference solutions (3 mL) were scanned at 200–380 nm and 10 μL of the DNA solution was subsequently added to both solutions. After 5 min, the absorbance was measured by scanning. This step was repeated

until the isoelectric point changed, indicating that the complex reacted completely with DNA.

Gel electrophoresis analysis

First, 1.25×10^{-5}, 2.5×10^{-5}, and 5×10^{-5} mol/L complex solutions were prepared along with a 0.1 mg/mL EB solution. Agarose gel was prepared by accurately weighing 1.5 g agarose in a 500 mL beaker, adding 1 mL of newly prepared EB dye, and slowly adding 180 mL of TAE buffer. Then, 1 μL of pBR322 DNA solution and 6 μL of the samples with different concentrations were mixed. After 2 h of reaction, 2 μL of the loading buffer was added and mixed evenly. The electrophoresis tank was connected and set to 80 V and 500 mA for 110 min. Finally, a gel image analyser was used for observation and photography.[29]

MTT colorimetric assay

The cell culture medium with optimal growth characteristics was selected, 2 mL trypsin was added along with 1 mL of culture medium, mixed, and the 96-well plate was covered. After a day, the 100, 50, 25, 12.5, and 6 μg/mL complex solutions were prepared. The original culture medium was precipitated and 200 μL of the complex solution was added and incubated for 72 h. The 1 mg/mL MTT solution was prepared, and the culture medium in the original well was precipitated. The 200 μL MTT culture medium was added and the cells were cultured for 4 h. The MTT colour solution (150 μL DMSO) was then added and the absorbance at 490 nm was measured using a microplate reader.

Flow cytometry evaluation

BxPC-3 cells were inoculated into the medium and placed in a carbon dioxide incubator for 24 h. A solution of 100 μg/mL copper and cobalt complexes was injected into different culture flasks. After 24 h, the supernatant was discarded and 1 mL of pancreatic digestive enzyme containing EDTA was added. The cell suspension was mixed, transferred into a 2 mL centrifuge tube, and centrifuged. The supernatant was removed and the cells were washed twice with phosphate buffered saline (PBS). Then, 100 μL of binding buffer was injected into the centrifuge tube and mixed again. Subsequently, 5 μL of Annexin V-FITC and 5 μL of PI was added to the centrifuge tube in the dark and left for 15 min. Binding buffer (400 L) was added filtered with a 300 mesh filter cloth before detection and analysis by flow cytometry (Accuri C6).

Cell fluorescence imaging studies

Two BxPC-3 cell culture media at appropriate and equal densities were prepared in six-well plates. After treatment with 200 μg/mL complex for 24 h, the cell culture medium was rinsed with 200 μL PBS and stained with 400 μL calcein. After 5 mins, 400 μL PI dye was added and rinsed with 200 μL PBS. Another medium was taken, and 200 μL PBS was added to remove excess dead cells, and 200 μL of cell tissue fluid was fixed for 15 min. After removing the cell fixative, 400 μL of the DAPI dye was added to the cell culture medium, and excess dye was washed with 400 μL PBS. After allowing the cells to stand for 15 min, they were photographed and observed under an inverted fluorescence microscope.

Acknowledgements

This work was supported financially by Liao Ning Revitalization Talents Program (XLYC1907047), Liaoning Science and Technology Project Management (grant number, 2020-YKLH-40, 2021-BS-185). Scientific Research Fund of Shenyang Medical College (20201004, 20191023).

Conflict of Interests

The authors declare no conflict of interest.

Data Availability Statement

The data that support the findings of this study are available from the corresponding author upon reasonable request.

Keywords: Anticancer · Apoptosis · Cytotoxicity · DNA binding · Fluorescence spectra

[1] B. P. Yuan, J. Y. Hu, Y. Guo, J. S. Zhang, S. Zhang, K. Y. Zhang, J. A. Zhao, H. W. Hou, *J. Poly.* **2021**, *203*, 115225.
[2] K. Karidi, A. Garoufis, N. Hadjiliadis, M. Lutz, A. L. Spek, J. Reedijk, *Inorg. Chem.* **2006**, *45*, 10282–10292.
[3] Y. M. Chen, Y. C. Liu, J. Q. Wang, G. C. Ou, X. F. Wang, S. Q. Gao, K. J. Du, Y. W. Lin, *J. Inorg. Biochem.* **2023**, *247*, 112330.
[4] X. R. Song, W. M. Li, J. N. Xu, P. Ji, Y. C. Li, G. D. Feng, B. Wang, *Anal. Chem.* **2023**, *95*, 3883–3891.
[5] N. H. Truong-Thi, N. H. Nguyen, D. T. D. Nguyen, T. N. Tang, T. H. Nguyen, D. H. Nguyen, *Eur. Polym. J.* **2023**, *185*, 111818.
[6] S. P. Basourakos, L. Li, A. M. Aparicio, P. G. Corn, J. Kim, T. C. Thompson, *Curr. Med. Chem.* **2017**, *24*,1586–1606.
[7] D. S. Goodsell, *Oncologist.* **2006**, *11*, 316–317.
[8] S. Ghosh, *Bioorg. Chem.* **2019**, *88*,102925.
[9] W. Lu, J. Y. Tang, Z. Z. Gu, L. Sun, H. M. Wei, Y. Q. Wang, S. L. Yang, X. W. Chi, L. Xu, *J. Inorg. Biochem.* **2023**, *238*, 112030.
[10] P. C. Bruijnincx, P. J. Sadler, *Curr. Opin. Chem. Biol.* **2008**, *12*, 197–206.
[11] Y. Jung, S. J. Lippard, *Chem. Rev.* **2017**, *107*, 1387–1407.
[12] K. Tishchenko, E. Beloglazkina, M. Proskurnin, V. Malinnikov, D. Guk, M. Muratova, O. Krasnovskaya, A. Udina, D. Skvortsov, R. R. Shafifikov, Y. Ivanenkov, V. Aladinskiy, I. Sorokin, O. Gromov, A. Majouga, N. Zyk, *J. Inorg. Biochem.* **2017**, *175*, 190–197.
[13] S. van Zutphen, J. Reedijk, *J. Coord. Chem. Rev.* **2005**, *249*, 2845–2853.
[14] H. S. NagendraPrasad, A. P. Ananda, S. Najundaswamy, S. Nagashree, P. Mallu, B. P. Dayananda, H. S. Jayanth, P. Mallu, *J. Mol. Struct.* **2021**, *17*, 130047.
[15] X. B. Fu, D. D. Liu, Y. Lin, W. Hu, Z. W. Mao, X. Y. Le, *Dalton Trans.* **2014**, *43*, 8721.
[16] Y. H. Xi, X. Yan, F. Bigdeli, Q. W. Zhang, L. L. Esrafili, Y. Hanifehpour, W. B. Zhang, M. L. Hu, A. Morsali, *Appl. Organomet. Chem.* **2022**, *36*, e6458.
[17] H. Tapiero, D. M. Townsend, K. D. Tew, *Biomed. Pharmacother.* **2003**, *57*, 386–398.
[18] B. E. Kim, T. Nevitt, D. J. Thiele, *Nat. Chem. Biol.* **2008**, *4*, 176–185.
[19] S. A. Shaikh, S. S. Bhat, V. K. Revankar, B. D. Kulkarni, K. Kumara, N. K. Lokanath, V. Kumbar, K. Bhat, R. J. Butcher, *ChemistrySelect* **2021**, *6*, 12666–12676.
[20] J. R. Sorenson, *Prog. Med. Chem.* **1989**, *26*, 437–568.
[21] B. Ebenezer, K. Nagashri, *Nucleos Nucleot Nucl.* **2021**, *40*, 1159–1197.
[22] M. Baldini, M. B. Ferrari, F. Bisceglie, G. Pelosi, S. Pinelli, P. Tarasconi, *Inorg. Chem.* **2004**, *43*, 7170.
[23] M. K. Shanmugaiah, K. M. Palsamy, R. Lokesh, I. Gandhi, N. L. Mitu, R. Jegathalaprathaban, R. Gurusamy, *Appl. Organomet. Chem.* **2018**, *33*, e4762.
[24] L. Tabrizi, F. Talaie, H. Chiniforoshan, *J. Biomol. Struct. Dyn.* **2017**, *35*, 3330–3341.

[25] X. Zhang, C. Bi, Y. Fan, Q. Cui, D. Chen, Y. Xiao, Q. P. Dou, *Int. J. Mol. Med.* **2008**, *22*, 677.
[26] S. Baskaran, M. M. Krishnan, M. N. Arumugham, *J. Coord. Chem.* **2015**, *68*, 4395–4407.
[27] P. D. Bonnitcha, B. J. Kim, R. K. Hocking, J. K. Clegg, P. Turner, S. M. Neville, T. W. Hambley, *Dalton Trans.* **2012**, *41*, 11293–11304.
[28] S. Mukherjee, H. Dinda, L. Shashank, I. Chakraborty, R. Bhattacharyya, J. Das Sarma, R. Shunmugam, *Macromolecules* **2015**, *48*, 6791–6800.
[29] Z. Ghasemian, D. Shahbazi-Gahrouei, S. Manouchehri, Avicenna *J. Med. Biotechnol.* **2015**, *7*, 64–68.
[30] N. Yamamoto, A. K. Renfrew, B. J. Kim, N. S. Bryce, T. W. Hambley, *J. Med. Chem.* **2012**, *55*, 11013–11021.
[31] A. K. Renfrew, N. S. Bryce, T. W. Hambley, *Chem. Sci.* **2013**, *4*, 3731–3739.
[32] M. Valko, M. Izakovic, M. Mazur, C. J. Rhodes, J. Telser, *Mol. Cell. Biochem.* **2004**, *266*, 37–56.
[33] L. J. K. Boerner, J. M. Zaleski, *Curr. Opin. Chem. Biol.* **2005**, *9*, 135–144.
[34] K. Radhakrishnan, T. Khamrang, K. Sambantham, V. K. Sali, U. Chitgupi, J. F. Lovell, A. A. Mohammad, R. Venugopal, *Polyhedron* **2021**, *194*, 114886.
[35] Z. F. Zeng, Q. P. Huang, J. H. Cai, G. J. Zheng, Q. C. Huang, Z. L. Liu, Z. L. Chen, Y. H. Wei, *Molecules* **2021**, *26*, 4028.
[36] A. I. B. Romo, M. P. Carepo, P. Levín, O. R. Nascimento, D. E. Díaz, J. R. López, I. E. León, L. F. Bezerra, L. Lemus, I. C. N. Diógenes, *Dalton Trans.* **2021**, *50*, 11931–11940.
[37] Y. Thakur, R. Agrawal, M. Tripathi, M. K. Siddiqi, E. Mohapatra, R. H. Khan, R. Pande, *J. Mol. Struct.* **2019**, *1197*, 691–706.
[38] L. Tabrizi, M. Fooladivanda, H. Chiniforoshan, *BioMetals* **2016**, *29*, 981–993.
[39] T. Ma, J. Xu, Y. Wang, H. Yu, Y. Yang, Y. Liu, W. L. Ding, W. J. Zhu, R. H. Chen, Z. J. Ge, Y. F. Tan, L. Jia, T. F. Zhu, *J. Inorg. Biochem.* **2015**, *144*, 38–46.
[40] D. B. Sloan, J. M. Warren, A. M. Williams, S. A. Kuster, E. S. Forsythe, *Genome Biol. Evol.* **2022**, *355*, e2100408.
[41] K. Busra, Y. Zehra Kubra, S. Onur, A. Belma, U. Bahri, *New J. Chem.* **2020**, *44*, 9313.
[42] G. Hamid, Y. Somaieh, T. Yune Abbasi, D. Michal, E. Vaclav, *RSC Adv.* **2022**, *12*, 13580.
[43] M. R. Rodríguez, M. J. Lavecchia, B. S. Parajón-Costa, A. C. González-Baró, M. R. González-Baró, E. R. Cattáneo, *J. Biochem.* **2021**, *186*, 43–50.
[44] I. Muhammad, U. Amir, H. Ihsan, A. Muhammad, T. Saqib, N. Muhammad, M. Syed, *J. Coord. Chem.* **2021**, *74*, 762–778.
[45] W. Zhao, V. Ferro, M. V. Baker, *Coord. Chem. Rev.* **2017**, *339*, 1–16.
[46] A. Regiel-Futyra, J. M. Dabrowski, O. Mazuryk, K. Spiewak, A. Kyziol, B. Pucelik, M. Brindell, G. Stochel, *Coord. Chem. Rev.* **2017**, *351*, 76–117.
[47] K. Venkateswarlu, S. Daravath, G. Ramesh, P. Lakshmi, Shivaraj, *Appl. Organomet. Chem.* **2021**, *35*, e6326.
[48] Z. Marwa, M. Mashaly, S. Mona, F. Rania, *Appl. Organomet. Chem.* **2023**, *37*, e7003.
[49] X. X. Ji, X. P. Zhu, S. Y. Chen, D. X. Song, S. Y. Wu, Y. Zhang, E. J. Gao, J. Xue, M. C. Zhu, *J. Solid State Chem.* **2022**, *305*, 122707.
[50] M. C. Zhu, X. X. J, S. L. Wang, H. H. Bao, H. S. Li, E. J. Gao, S. Y. Wu, J. Wang, Q. Chen, J. Xu, X. P. Zhu, *Inorg. Chem. Commun.* **2021**, *128*, 10857.
[51] T. Zandvakili, S. Jamil Fatemi, S. Yousef Ebrahimipour, H. Ebrahimnejad, J. Castro, M. Dusek, V. Eigner, *J. Mol. Struct.* **2022**, *1249*, 131525.
[52] S. A. Elsayed, I. M. Elnabky, A. D. Biase, A. M. El-Hendawy, *Appl. Organomet. Chem.* **2002**, *36*, e6481.
[53] M. Deiana, B. Mettra, K. Matczyszyn, D. Pitrat, M. Samoc, *ACS. Biomac.* **2016**, *17*, 3609–3618.
[54] M. C. Zhu, W. Ning, M. B. Meng, J. Q. Su, T. T. Peng, Z. Z. Qi, B. Jia, Y. H. Feng, E. J. Gao, *Appl. Organomet. Chem.* **2018**, *32*, e4571.

Manuscript received: July 22, 2023